

SI Appendix

Inducing protein aggregation by extensional flow

John Dobson, Amit Kumar, Leon F. Willis, Roman Tuma, Daniel R. Higazi, Richard Turner,
David Lowe, Alison E. Ashcroft, Sheena E. Radford, Nikil Kapur, and David J. Brockwell

Supplementary method

CFD

The CFD package used for this study is COMSOL 4.3b which employs a finite element method. The fluid properties used in the model were those of water at 20 °C (predefined within the CFD package) as protein solutions were prepared at low enough concentrations so as to have negligible effect on fluid viscosity (1). The pertinent geometry of the constriction region where the extensional flow field occurs is shown Figure 1 in three-dimensions; judicious choice of boundary conditions allows this to be modelled as a 2-dimensional slice in an axial co-ordinate system (Figure 1 D(i)) without the loss of any of the underlying physics but with the advantage of reducing the scale of the computational problem. The inlet is specified as a fully developed laminar flow (flow through the device is slow with low Reynolds number, $Re \ll 2000$, see below) with a specified volumetric flow rate that is chosen to match that created by the piston movement within the syringe body. The outlet is defined as a pressure condition, and is located far enough downstream of the constriction to prevent back-flow into the domain. The bottom edge of the domain represents the axis of symmetry of the problem and the axis about which the slice is rotated about to give the fully reconstructed domain. Axial symmetry was defined about the radial axis $r = 0$. A no slip boundary condition was enforced on all of the remaining vertices in the model. The mesh was a relatively fine quadrilateral mesh with uniform finite elements making up the main bulk of the model and finer elements at the walls to give accurate non-slip boundary conditions. Lack of sensitivity of the solution to the mesh was confirmed.

The general steps of defining the geometry (using the parameters shown in Table S1), applying boundary conditions, discretising the domain into a grid structure and solving the flow field are followed, with checks made that the grid density is high enough to resolve the problem

accurately. From a characterization perspective, the laminar Navier-Stokes equations in an axisymmetric coordinate system are solved to characterize the flow in terms of the velocity and pressure at each point, which can then be interpreted in terms of the shearing and extensional flow field. The flow exponent n ($Q = k\Delta P^n$, where Q is the flow rate, ΔP is the pressure drop and k is the flow coefficient of units $\text{m}^3\text{s}^{-1}\text{Pa}^n$) was calculated to determine the dominant flow regime; where $n = 1$ is laminar and $n = 0.5$ is turbulent. For our device, $n = 0.905$ and thus generates a predominantly laminar flow. In accordance with this, the Reynolds Number was found to be $\ll 2000$ throughout the device (Table S1).

Reynolds number

Reynolds number was calculated by:

$$Re = \frac{\rho u L}{\mu}$$

Where ρ is the fluid density, u the fluid velocity, L a characteristic length scale (in this case the pipe diameter) and μ is the dynamic viscosity.

Extensional flow

Strain ε is a measure of mechanical extension given by $\varepsilon = \frac{l' - l}{l}$ where l is the original length and l' is the extended length. Therefore rate of strain $\dot{\varepsilon}$ is the time derivative of ε . Along the axis the centre-line strain is given by $\dot{\varepsilon}_{c-l} = \frac{du}{dx}$. More generally, the strain rate field is calculated following the deformation tensors described in (2)

Calculating Hydraulic Energy

The energy applied to a unit sphere as it passes through the contraction is calculated as $E_s = \frac{P_h V_s}{\dot{Q}}$ where V_s is the sphere volume, \dot{Q} is the volumetric flow rate and P_h is the hydraulic power.

The hydraulic power is calculated from $P_h = \dot{Q} \Delta P$ where ΔP is either the pressure drop over the contraction or capillary. The pressure drop is taken from the CFD simulation.

Model used to estimate extensional force

The force applied onto a protein molecule was estimated using the “elementary model for shear denaturation of a protein by elongational flow” (Figure 7, ref (3)). The protein model used in our calculations comprised 583 residues configured as a dumbbell of two spheres each containing 2/5 of the residues, joined by the remaining residues in an extended conformation.

Operation of extensional flow device

The syringes were aligned and secured using a ThorLabs optics board. A screw-jack linear actuator attached to two shunts was used to depress the syringe plungers. The actuator was driven by a single stepper motor to allow for accurate flow rate and volume control.

The protein solution was shuttled between the two syringes along the capillary tube as seen in (Figure 1). The syringe plungers are linked hydraulically through the protein solution such that, as one syringe plunger is depressed, the fluid forces cause the other to be expelled from its syringe jacket. The stepper motor was controlled directly by an embedded microcontroller maintaining a constant velocity throughout the experiment. Prior to each experiment, the syringes were flushed with 2 % (v/v) Hellmanex-III solution and MilliQ-grade H₂O, followed

by a final wash with 0.22 μm -filtered and de-gassed buffer. 500 μL of 0.22 μm -filtered protein solution was drawn into one syringe very slowly through the capillary so as not to damage the protein prematurely. Any bubbles were expelled and then the other end of the capillary attached to the second empty syringe (pre-secured to the optics board with the plunger fully depressed to eliminate air from the system), sealed with the compression fitting and the first syringe clamped in place.

Purification of G-CSF C3

Cell pellets were resuspended in lysis buffer (50 mM TrisHCl, 5 mM EDTA, 2 mM phenylmethanesulphonyl fluoride (PMSF) and 2 mM benzamidine hydrochloride hydrate pH 8) at a ratio of 1 g of cell pellet to 10 mL of buffer and lysed by 5 \times 30 second periods of sonication on ice at 75 % amplitude, using a Sonics Vibra-Cell™ VCX-130PB sonicator with a 6 mm diameter probe. Inclusion bodies were harvested by centrifugation at 15000 rpm, 4 °C for 30 mins, using a Beckman Coulter Avanti J-26 XP centrifuge with JLA 16.250 rotor. Inclusion bodies were then washed by re-suspending in wash buffer 1 (50 mM TrisHCl, 5 mM EDTA, 1 % (v/v) triton X-100 pH 8) at a ratio of 1 g of inclusion body pellet to 20 mL of buffer and harvesting inclusion bodies by centrifugation as before. This wash step was repeated using wash buffer 2 (50 mM TrisHCl, 5 mM EDTA, 4 M urea pH 8). Washed inclusion bodies were resuspended in unfolding buffer (50 mM TrisHCl, 5 mM EDTA, 6 M GdnHCl, 10 mM DTT pH 8) at a ratio of 1 g of inclusion body pellet to 5 mL of buffer and left shaking overnight. The resuspended pellet was then centrifuged at 15000 rpm, 4 °C for 1 h, using a Beckman Coulter Avanti J-26 XP centrifuge with JA 25.50 rotor. The supernatant was diluted 1 in 10 with refolding buffer (50 mM TrisHCl, 5 mM EDTA, 0.9 M L-arginine pH 8) and immediately dialysed into 5 L of 20 mM sodium phosphate, 20 mM sodium acetate pH 4. After three dialysis

changes refolded G-CSF was centrifuged at 15000 rpm for 30 mins as above and the supernatant filtered through a 0.22 μm filter. The filtrate was loaded onto a 5 mL HiTrapTM SP HP cation exchange column (GE Healthcare) at a flow rate of 5 mL min⁻¹ using an Äktaprime plus (GE Healthcare) system. A gradient of 0-100 % elution buffer (20 mM sodium phosphate, 20 mM sodium acetate, 1 M NaCl pH 4) was then run over 100 mL, with 2 mL fractions being collected. Fractions were pooled based on the results of SDS-PAGE analysis and desalted by dialysis as above. After desalting, pools were concentrated using Vivaspin 20 centrifugal concentrators with 5 kDa MWCO PES membrane (Sartorius Stedim) until the protein concentration was approx. 8-10 mg mL⁻¹ and snap frozen using dry ice and ethanol for storage at -80 °C.

Dynamic Light Scattering (DLS)

Protein samples at a range of concentrations (1-10 mg mL⁻¹) were stressed for a defined number of passes (10-2000 passes) in an appropriate buffer (see Methods). 5 mg mL⁻¹ samples were diluted 1:2 and 10 mg mL⁻¹ samples 1:5 with the same buffer to avoid saturating the detector. 250 μL samples were injected into a Wyatt miniDawnTreos[®] system (equipped with an additional DLS detector) and the data analyzed using Astra 6.0.3[®] software supplied with the instrument. Filtered (0.22 μm) and de-gassed buffer, kept cool on ice to minimize bubble formation inside the instrument, was used to obtain 5 min baselines before and after sample injection. A three minute sample window was used for the analysis by the software. The flow cell was flushed with 1 mL each of 0.22 μm filtered and degassed 1 M nitric acid and MilliQ-grade H₂O after each run, followed by 2 mL of buffer. Correlation curves were analyzed using the Astra 6.0.3 software by the methods of regularization (4) and, where appropriate, cumulants analysis (5, 6). The latter method extracts the Z-average radius (z) and standard deviation (σ)

of a polydisperse solution (6). These parameters were then used to calculate the polydispersity index (PDI):

$$PDI = \left(\frac{\sigma^2}{z^2} \right)$$

Nanoparticle Tracking Analysis (NTA)

Native and stressed protein samples were diluted in the same ratios as described for the DLS experiments to minimize noise in the instrument. A Nanosight® LM10 (Malvern Instruments) equipped with a 642 nm laser was used and the resultant data analysed using NTA 2.3 software. 250 µL protein solution was injected into the sample chamber, ensuring no air entered the system. Three, 90 s videos were recorded, analyzed and averaged in the software for each sample. The instrument parameters were set as follows: screen gain = 1, detection threshold = 10 nm, T = 22 °C, viscosity = 0.95 cP and camera brightness = 4-12 to minimise background noise. Particle size in NTA corresponds to the hydrodynamic diameter of the particles in nanometres. A 70 % (v/v) ethanol solution was used to clean the device between samples and an air-duster used to remove residual traces of ethanol from the inlets and O-ring followed by a buffer wash of the sample chamber prior to sample loading. The data were processed using Microsoft Excel® 2010 and plotted using Origin Pro® 8.6.

Transmission Electron Microscopy

20 µL protein solution (5 and 10 mg mL⁻¹ samples were diluted 1:2 or 1:5 with their respective buffer) was deposited onto carbon-coated EM grids for 45 seconds at room temperature. Excess sample was blotted onto filter paper and the grid washed with 3 × 20 µL of H₂O, followed by

staining in 10 μL of 2 % (w/v) uranyl acetate solution. Excess stain was removed by blotting and the grid allowed to air-dry. The grids were imaged using a JEOL JEM1400® transmission electron microscope at 120 kV. Images were recorded at 1000 \times and 10,000 \times magnification for each specimen using the AMT Image Capture Engine software Version 6.02 supplied with the instrument.

Fluorescence Correlation Spectroscopy

1 mg mL⁻¹ BSA solution (25 mM Tris.HCl pH 7.5 4 M urea) was mixed 1:10 (mol:mol) with sulfhydryl reactive dye (Alexa Fluor 488 C5 Maleimide, Molecular Probes) and allowed to conjugate for 4 h at room temperature. Unreacted dye was removed using a Superdex peptide column (10/300 GL, GE Healthcare). For the extensional flow experiment 10 μL (1 mg mL⁻¹) labelled BSA was added to the protein solution to be stressed (500 μL). After stressing, the protein solutions were analyzed on home-built FCS setup with confocal volume \sim 1 fL (7). Ten successive scans for 30 seconds were averaged to obtain a final correlation function. The data were analysed using a non-linear least squares method to fit to models accounting for one or two diffusing species alongside the triplet state using a home-written MATLAB scripts as described previously (8) and diffusion correlation times were converted into apparent hydrodynamic radii using calibration with free dye as described (9).

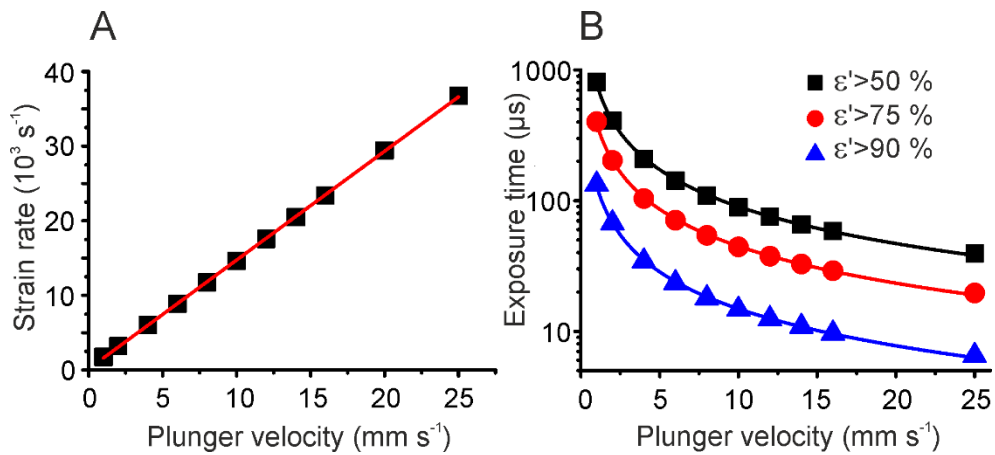


Figure S1: Centreline strain rate and corresponding exposure time in relation to plunger velocities of 1-25 mm s^{-1} calculated by CFD. (A) Centreline strain rate varies linearly with plunger velocity. Red line is a straight line fit to the data. (B) Relationship between plunger velocity and the time that a fluid element is exposed to a strain rate (ϵ') greater than 50 % (—), 75 % (—) or 90 % (—) of the maximum centreline strain rate. Lines are power-law fits to data ($R^2 > 0.995$ in all cases).

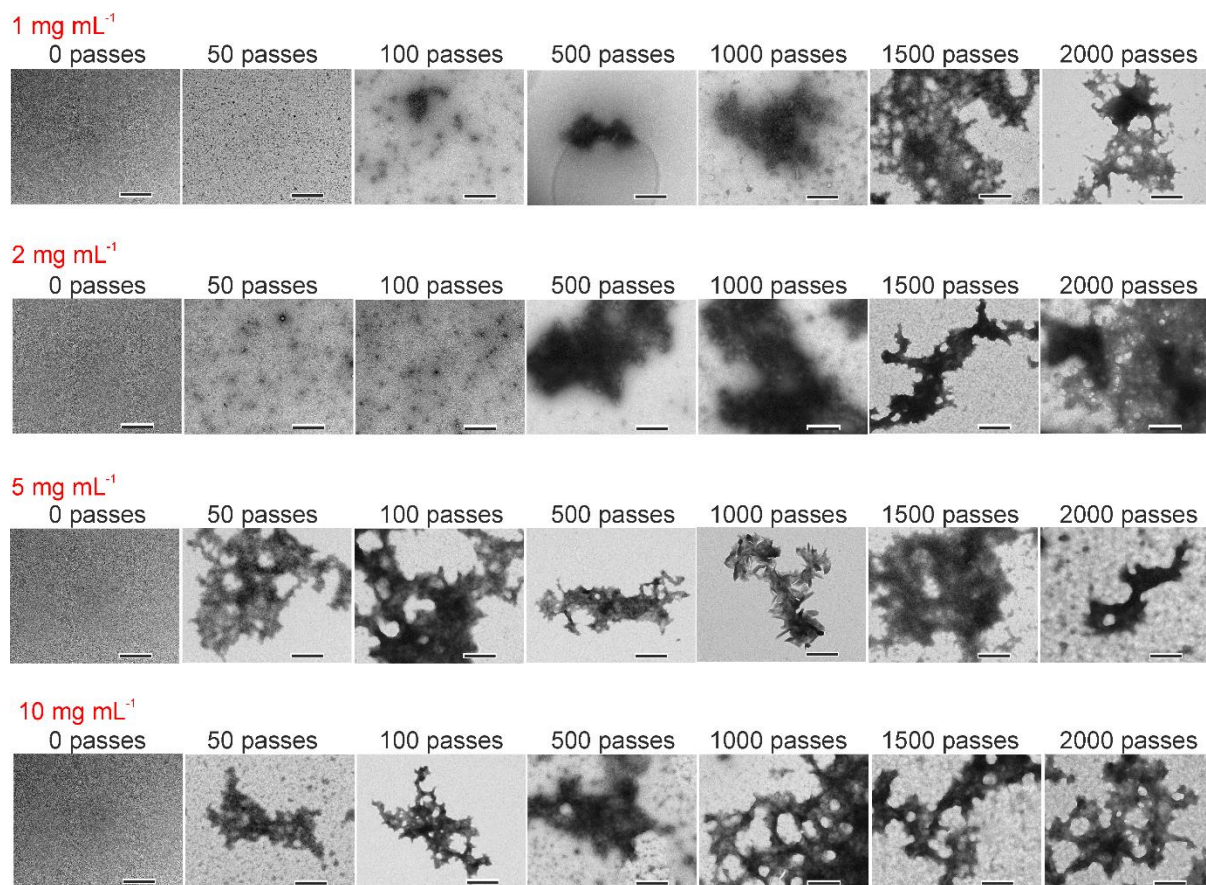


Figure S2: TEM images of BSA after extensional flow at the protein concentration and pass number stated. The plunger velocity in all experiments above was 8 mm s^{-1} (strain rate = 11750 s^{-1} , shear rate = 52000 s^{-1}). Images taken at $10000\times$ magnification, scale bar = 500 nm.

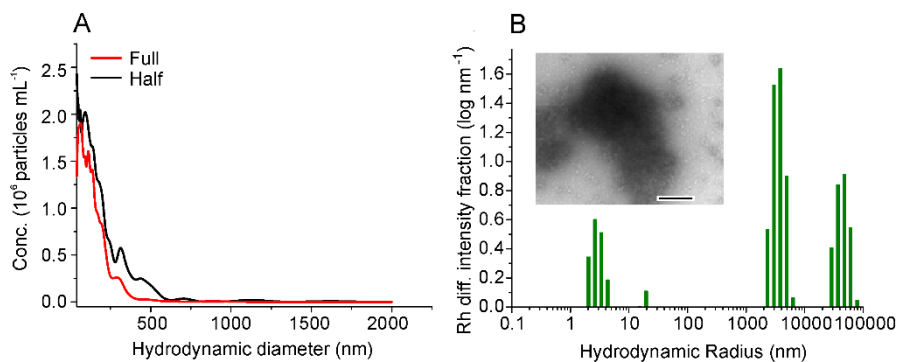


Figure S3: Control experiments under reduced shear by halving the capillary length. (A) Nanoparticle tracking analysis of BSA after 1000 passes through a half-length (**black**) or full-length (red) capillary. (B) Regularization plot of DLS data obtained for BSA after 1000 passes through a half-length capillary. Four distinct peaks were observed from left to right: $R_h = 2.9 \pm 0.7$ nm, 19.5 ± 1.5 nm, 3.6 ± 0.9 μm and 44.5 ± 11.9 μm . Inset: TEM image of BSA after 1000 passes. The image was taken at 10000 \times magnification, scale bar = 500 nm. In (A) and (B), the BSA concentration was 5 mg mL⁻¹ and the plunger velocity was 8 mm s⁻¹ (strain rate = 11750 s⁻¹ and shear rate = 52000 s⁻¹). Half-length capillaries were made by cleaving the full-length capillaries with a ceramic tile (Sutter Instruments) and finishing the cleaved capillaries in a Bunsen flame to remove sharp edges, before being used in experiments as stated in the main text.

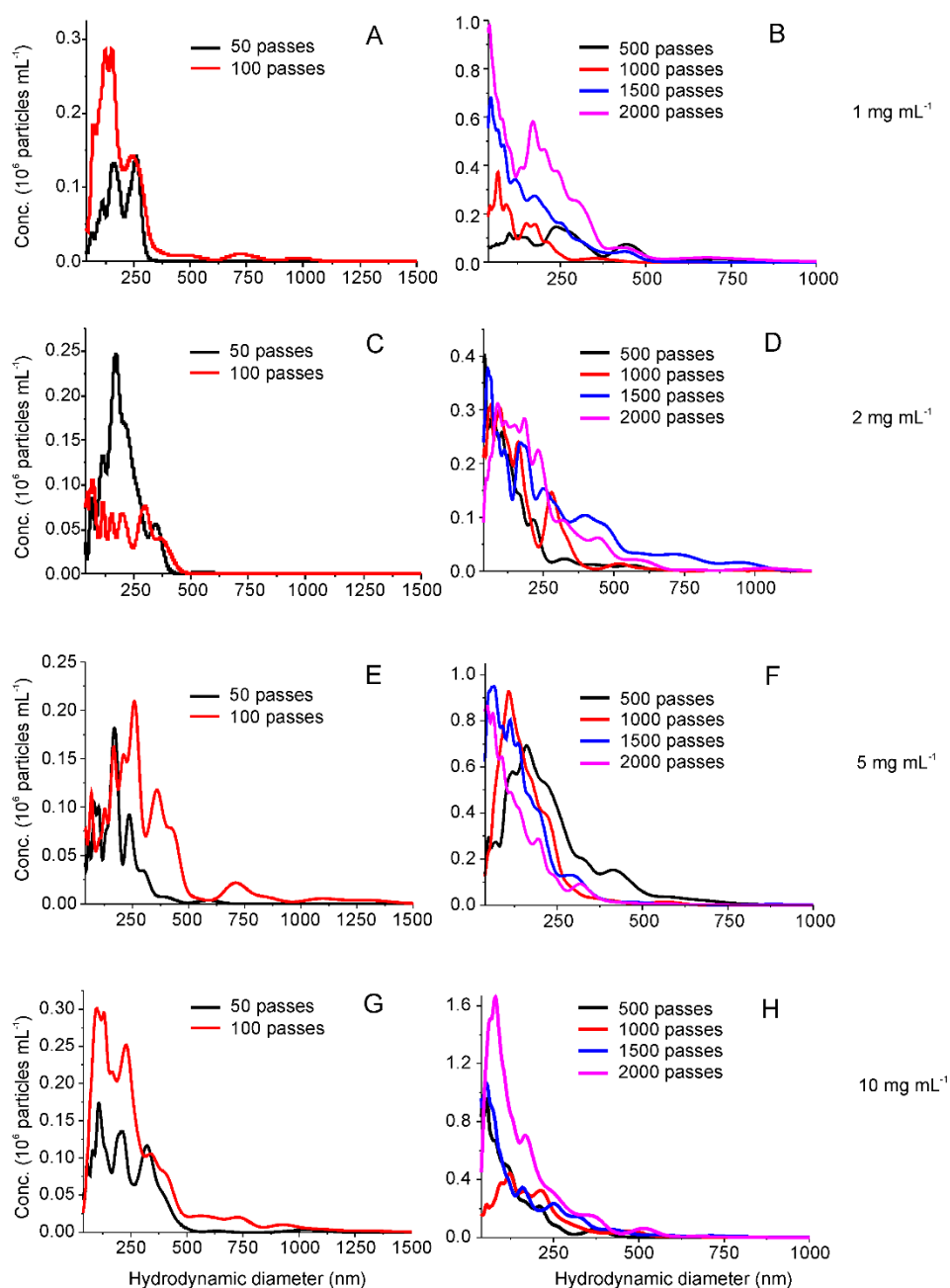


Figure S4: BSA aggregation analyzed by NTA. The experiments were performed at the number of passes indicated at different BSA concentrations. The plunger velocity in all cases was 8 mm s^{-1} (strain rate = 11750 s^{-1} and shear rate = 55200 s^{-1}). (A) and (B) at 1 mg mL^{-1} , (C) and (D) at 2 mg mL^{-1} , (E) and (F) at 5 mg mL^{-1} and (G) and (H) at 10 mg mL^{-1} of BSA. Note: very few or no aggregates (< 5 particles) were observed for BSA when fewer than 50 passes were applied, rendering the particle tracking analysis statistically invalid.

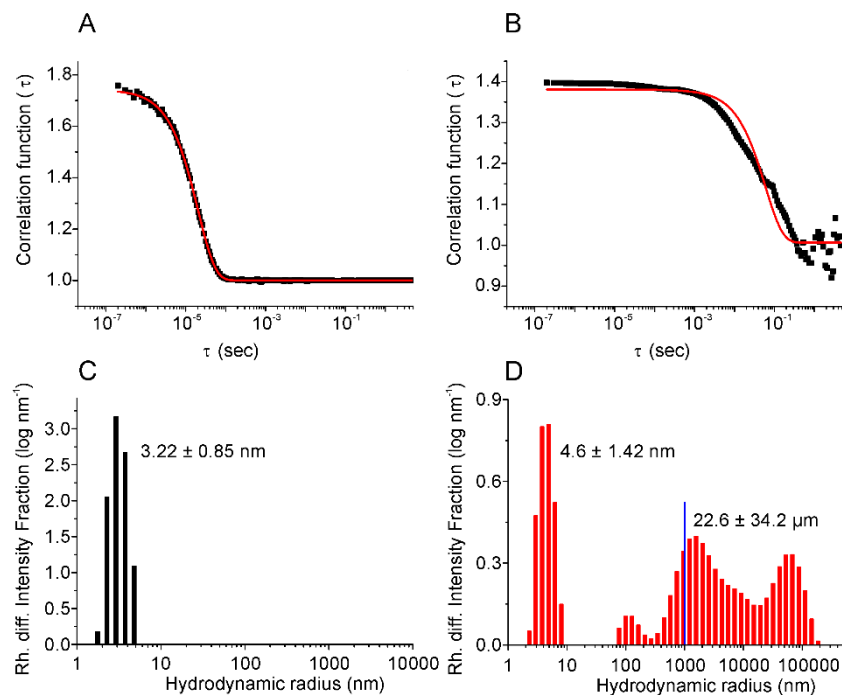


Figure S5: DLS correlation functions (black squares) of (A) native BSA and (B) BSA after 2000 passes of extensional flow stress. The BSA concentration in the experiment was 5 mg mL⁻¹, then diluted 1:2 with buffer prior to DLS injection (Supplemental Methods). Fitting a single exponential decay function (red line) to the correlation curve:

$$y = y_0 + Ae^{-x/\tau}$$

(where A is the amplitude, y_0 is a y axis off-set and τ is the delay time) yields a good fit for the native sample (monodisperse, $R^2 = 0.9997$) and a poor fit for BSA (disperse, $R^2 = 0.9719$) exposed to extensional flow, indicating the presence of two or more species. Data for poly-disperse samples were further analyzed by regularization (C and D) and cumulants analysis (Supplemental Methods). DLS regularization plots showing native BSA (C) and BSA after 2000 passes (D). Blue line at 1000 nm indicates the measurement limitation of the technique. In (A)-(D), the BSA solutions were passed through the extensional flow device at a plunger velocity of 8 mm s⁻¹ (strain rate = 11750 s⁻¹ and shear rate = 52000 s⁻¹).

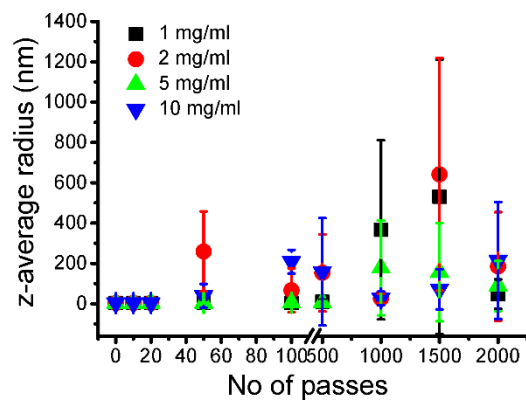


Figure S6: Plot of the z-average radii of 1, 2, 5 and 10 mg mL⁻¹ BSA as a function of pass number, obtained by cumulants analysis of the DLS data (Supplemental Methods). The plunger velocity was 8 mm s⁻¹ (strain rate = 11750 s⁻¹ and shear rate = 52000 s⁻¹). Error bars represent the error from two independent experiments except 2 mg/mL 1000 passes (N =1).

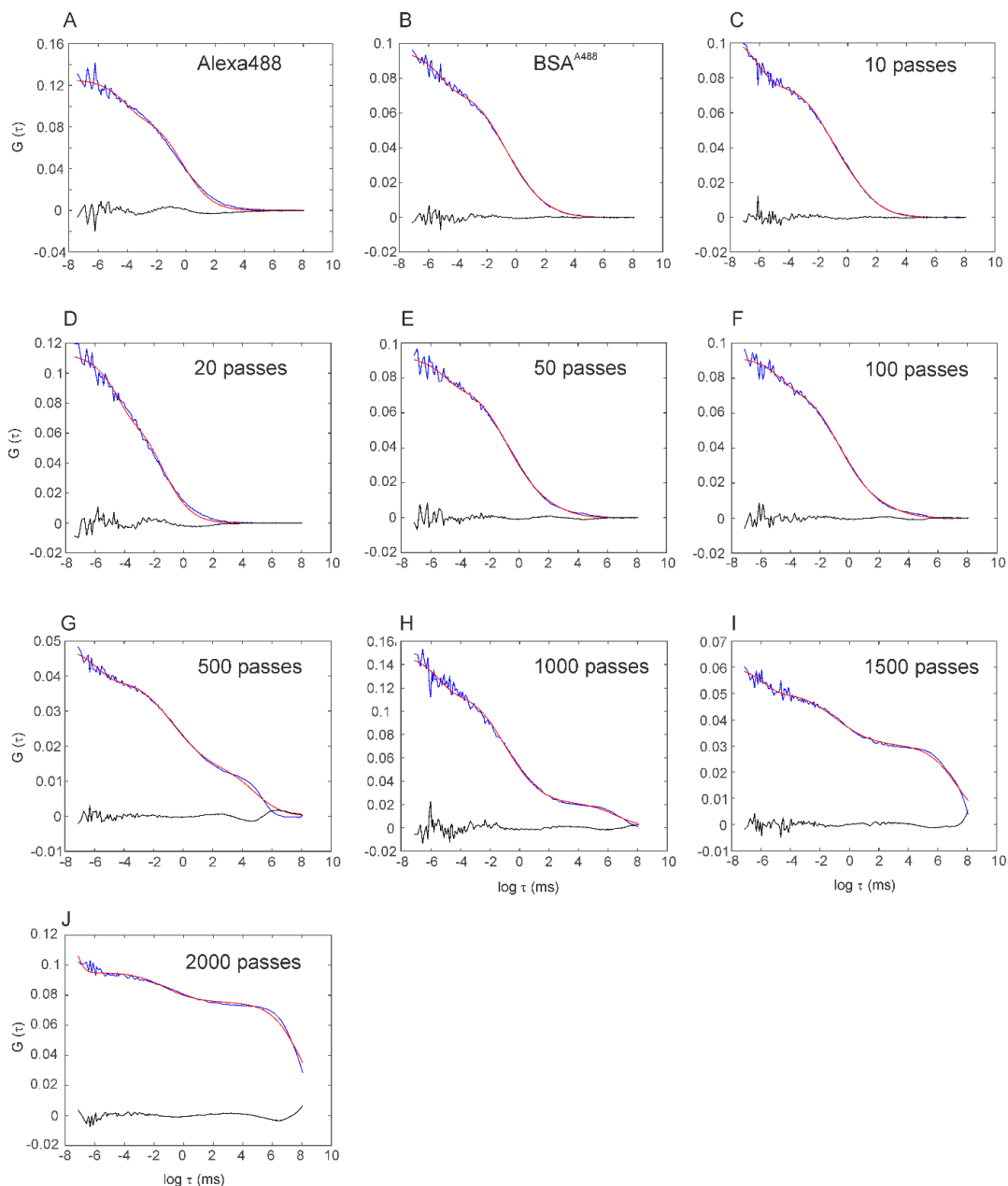


Figure S7: Aggregation of 5 mg mL^{-1} BSA solution after 10-2000 passes analyzed by FCS. Each plot shows the autocorrelation function (blue lines), their fits to a two component fit (red lines) and residuals (black lines). (A) Alexa-488 dye alone, single diffusion component (B) BSA-Alexa-488 prior to extensional strain, (C) after 10 passes, fitted to a single diffusion component model. Panels (D-J) show a two diffusion component fit of 20, 50, 100, 500, 1000, 1500 and 2000 passes, respectively. The plunger velocity was 8 mm s^{-1} (strain rate = 11750 s^{-1} and strain rate = 52000 s^{-1}).

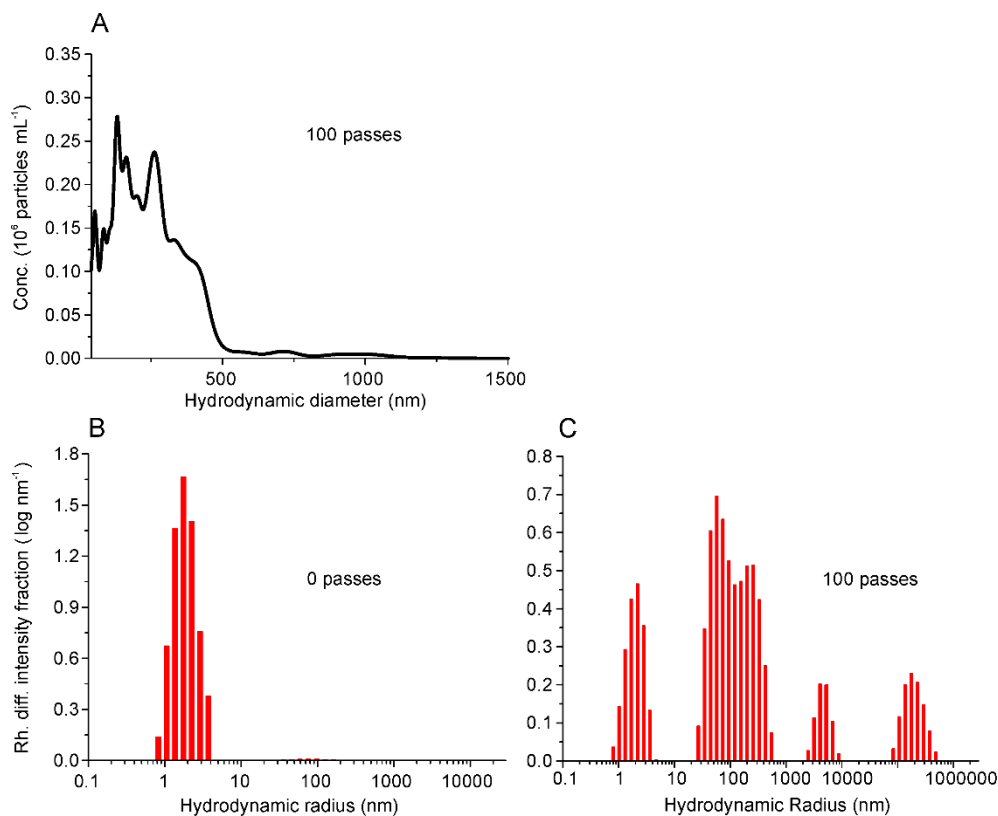


Figure S8: Analysis of extensional flow induced aggregation of 5 mg mL^{-1} $\beta_2\text{m}$ by NTA (A) and DLS (B and C). (A) NTA of 5 mg mL^{-1} $\beta_2\text{m}$ after 100 passes at a plunger velocity of 8 mm s^{-1} (strain rate = 11750 s^{-1}). Note: no aggregates were visible in the native (0 passes) sample or following 20 passes. (B) DLS regularization plot of native $\beta_2\text{m}$. The peak shows the mean $R_h = 2.5 \pm 0.1 \text{ nm}$, a value consistent with that determined using NMR (10). (C) DLS regularization plot of $\beta_2\text{m}$ after 100 passes of extensional flow at a plunger velocity of 8 mm s^{-1} (strain rate = 11750 s^{-1}). Four distinct peaks were observed from left to right: $R_h = 2.0 \pm 0.3$, 148 ± 13 , 4761 ± 125 and $207662 \pm 2261 \text{ nm}$. Cumulants analysis of the DLS data obtained PDI values of 0.21, 0.6 and 0.71 after 0, 20 passes and 100 passes, respectively.

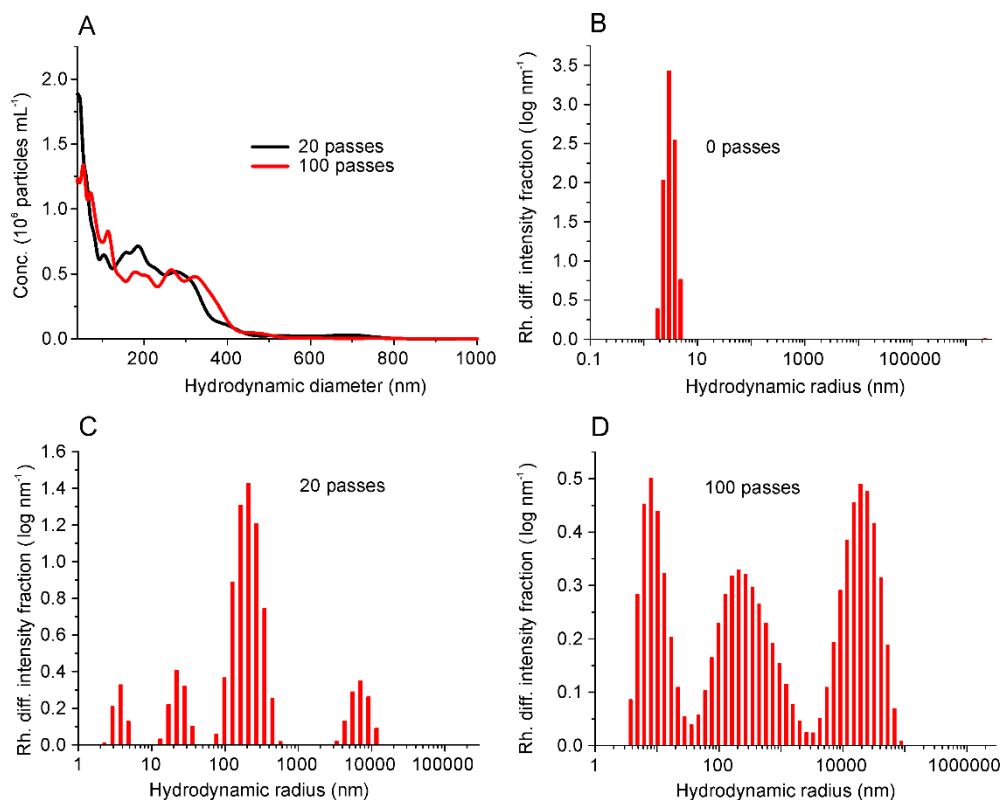


Figure S9: Analysis of extensional flow-induced aggregation of 0.5 mg mL^{-1} G-CSF C3 by NTA (A) and DLS (B-D). (A) NTA of G-CSF C3 subjected to extensional flow for 20 or 100 passes at a plunger velocity of 8 mm s^{-1} (strain rate = 11750 s^{-1}). Note: no particles/aggregates were observed in the native sample (0 passes). (B) DLS regularization plot of native G-CSF C3. A single dominant peak at $R_h = 3.5 \pm 0.8 \text{ nm}$ is observed. (C) DLS regularization plot of G-CSF C3 after 20 passes at the same velocity as in (A). Four distinct peaks were observed from left to right: $R_h = 3.7 \pm 0.2$, 24 ± 3 , 218 ± 5 , and $7091 \pm 19 \text{ nm}$. (D) DLS regularization plot of G-CSF C3 after 100 passes. The three apparent peaks observed were merged due to high sample dispersity precluding resolution into discrete peaks, with the mean $R_h = 8750 \pm 1400 \text{ nm}$. Cumulants analysis of the DLS data yields PDI values of >0.6 for both the 20 and 100 passes and < 0.1 for the native sample (0 passes).

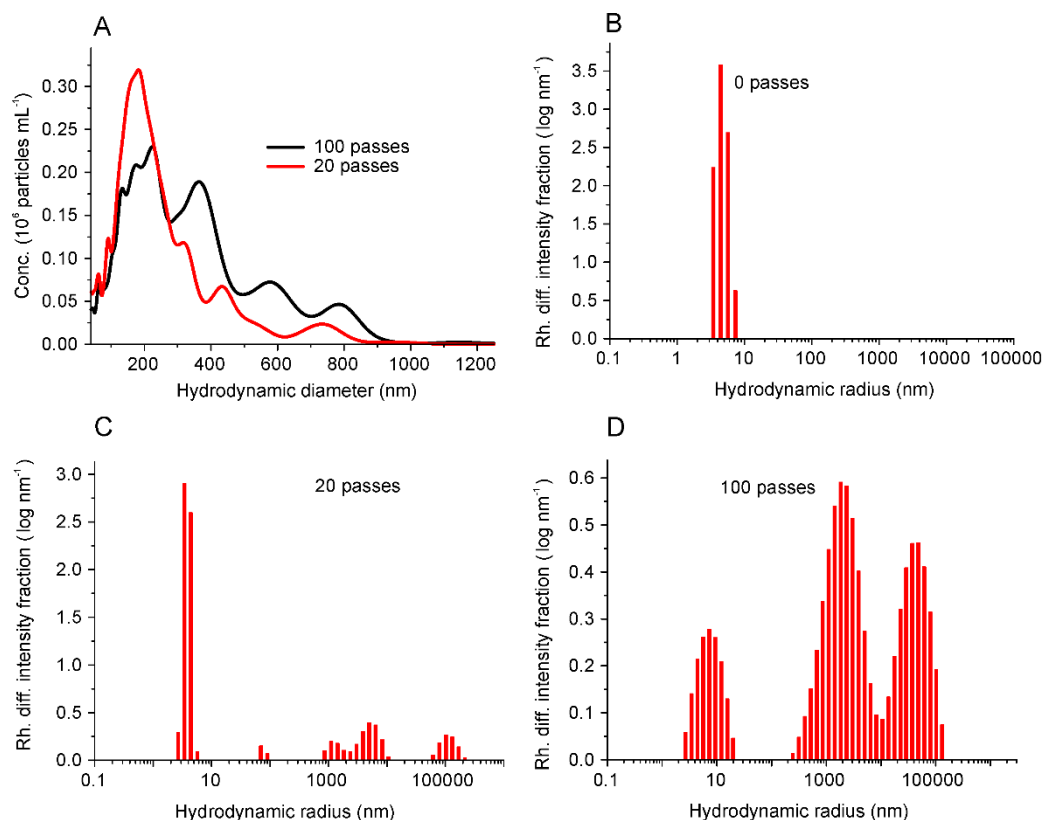


Figure S10: Analysis of extensional flow induced aggregation of 0.5 mg mL⁻¹ mAb1 by NTA (A) and DLS (B-D). (A) NTA of mAb1 subjected to extensional flow for 20 or 100 passes at a plunger velocity of 8 mm s⁻¹ (strain rate = 11750 s⁻¹). Note: the native protein (0 passes) did not contain any visible particles/aggregates. (B) DLS regularization plot of native mAb1. A single dominant peak at $R_h = 4.8 \pm 1.1$ nm is observed. (C) DLS regularization plot of mAb1 after 20 passes of extensional flow at the plunger velocity indicated in (A). Four peaks were observed from left to right: $R_h = 3.9 \pm 0.7$ nm, 76 ± 11 nm, 4.3 ± 2.5 μ m and 117.4 ± 37.1 μ m. (D) DLS regularization plot of mAb1 after 100 passes of extensional flow at the plunger velocity indicated in (A). The 1st peak (left) observed had a mean $R_h = 8.1 \pm 4.1$ nm, whilst the 2nd and 3rd peaks (right) were merged due to high sample dispersity precluding resolution into discrete peaks (mean $R_h = 20.3 \pm 1.0$ μ m). Cumulants analysis of the DLS data yields a PDI values of 0.1, > 0.6 and 0.4 for 0, 20 and 100 passes samples, respectively.

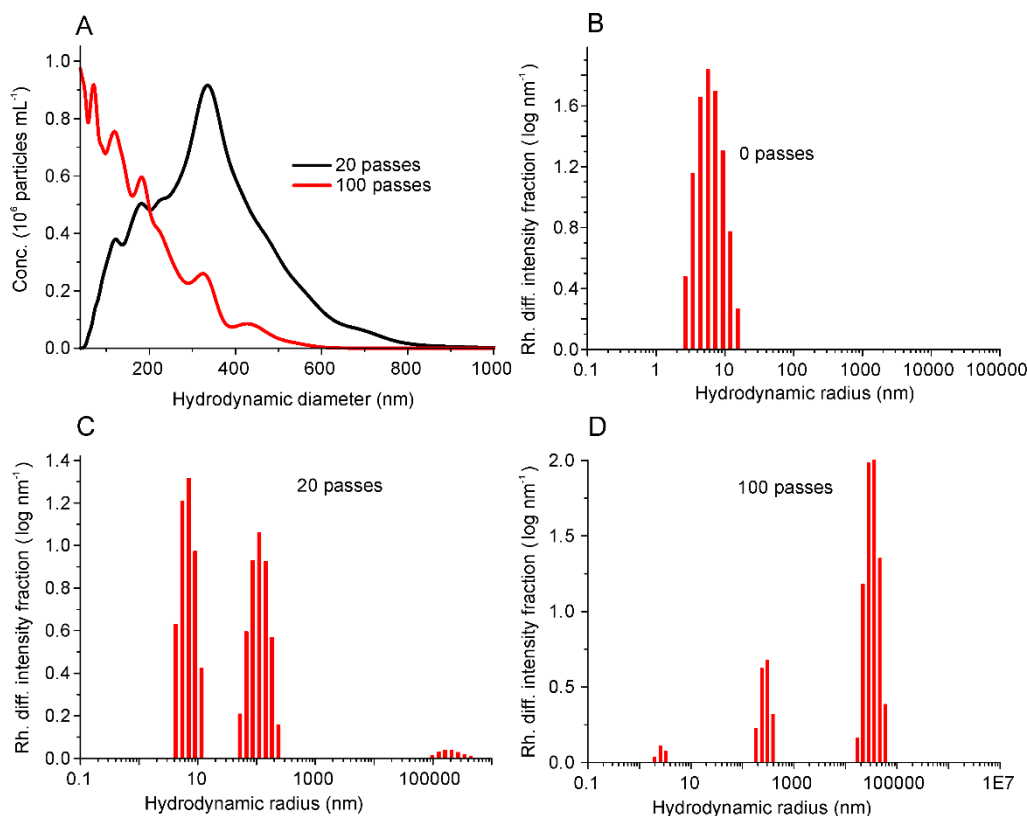


Figure S11: Analysis of extensional flow-induced aggregation of 0.5 mg mL⁻¹ MEDI1912_WFL by NTA (A) and DLS (B-D). (A) NTA of MEDI1912_WFL subjected to extensional flow for 20 or 100 passes at a plunger velocity of 8 mm s⁻¹ (strain rate = 11750 s⁻¹). Note: no particles/aggregates were visible in the native sample (0 passes). (B) DLS regularization plot for native MEDI1912_WFL. A single peak is observed, with $R_h = 6.61 \pm 3.04$ nm. (C) DLS regularization plot for MEDI1912_WFL for 20 passes at the plunger velocity indicated in (A). Three peaks are observed from left to right: $R_h = 7.05 \pm 2.2$ nm, 117.5 ± 44.9 nm and 212 ± 93.5 nm. (D) DLS regularization plot for MEDI1912_WFL for after 100 passes at the plunger velocity indicated in (A). Three peaks were observed from left to right: $R_h = 2.72 \pm 0.5$ nm, 281 ± 63.5 nm and 34.1 ± 10.6 nm. Cumulants analysis of the DLS data yields PDI values of 0.3 for the native sample (0 passes) and > 0.6 for both the 20 and 100 passes samples.

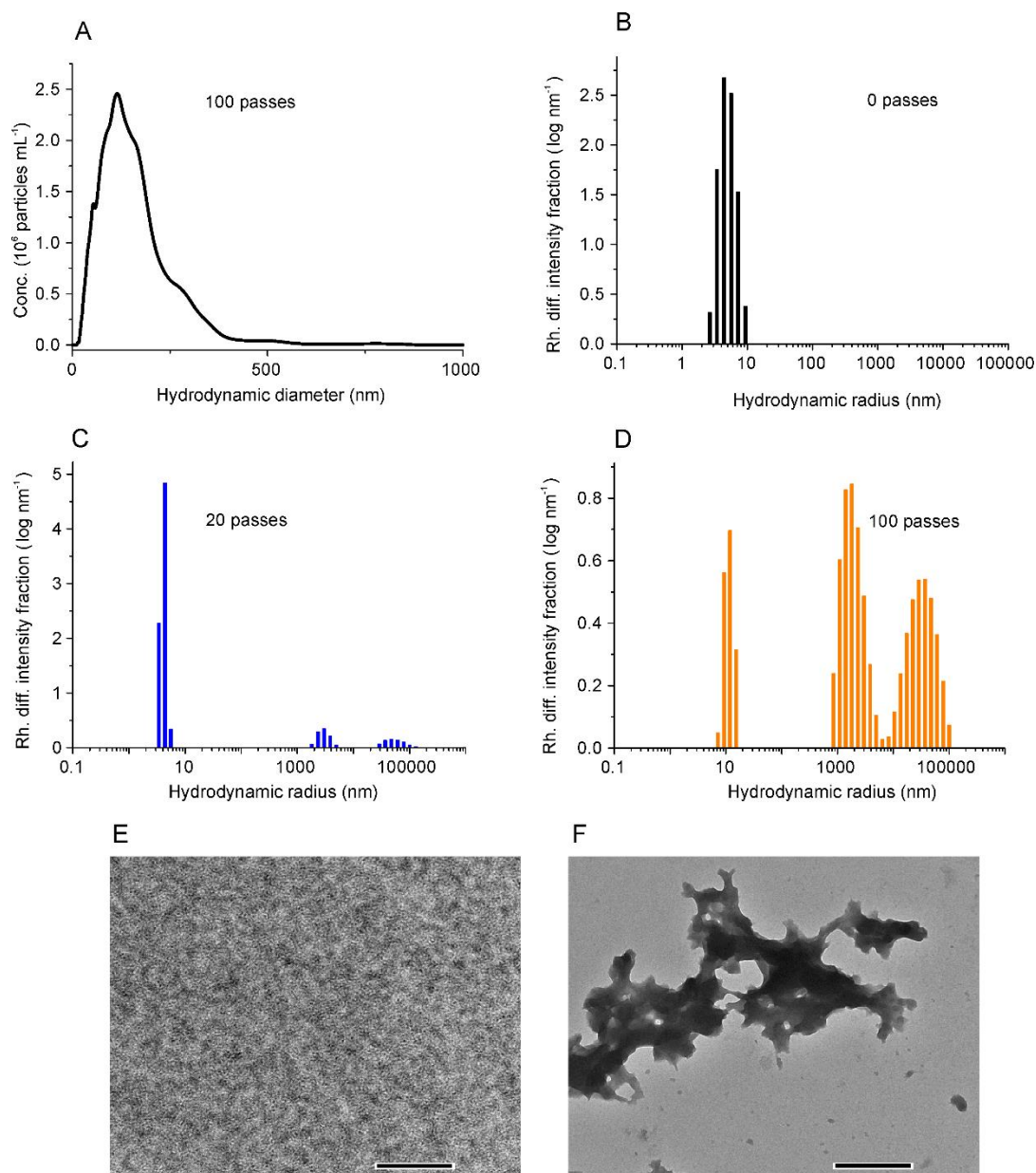


Figure S12 Analysis of extensional flow-induced aggregation of 0.5 mg mL^{-1} MEDI1912_STT by NTA (A) and DLS (B-D). (A) NTA of MEDI1912_STT subjected to extensional flow for 100 passes at a plunger velocity of 8 mm s^{-1} (strain rate = 11750 s^{-1}). Note: no particles/aggregates were detected in the native sample (0 passes). (B) DLS regularization plot for native MEDI1912_STT. A single peak is observed, with $R_h = 5.2 \pm 1.6 \text{ nm}$ (C) DLS regularization plot MEDI1912_STT after 20 passes at the plunger velocity indicated in (A). Three peaks are observed, with $R_h = 4.1 \pm 0.6 \text{ nm}$, $3.0 \pm 0.8 \mu\text{m}$ and $57.4 \pm 23.9 \mu\text{m}$ (D) DLS regularization plot for MEDI1912_STT after 100 passes. The 1st peak observed (left) had a

mean $R_h = 11.49 \pm 2.42$ nm, whilst the 2nd and 3rd peaks (right) were merged due to high sample dispersity precluding resolution into discrete peaks (mean $R_h = 17.84 \pm 22.24$ μ m). Cumulants analysis of the DLS data yield PDI values of 0.1, 0.3 and > 0.6 , for the 0, 20 and 100 passes samples, respectively. (E) TEM image of native MEDI1912_STT. (F) TEM image of MEDI1912_STT after 100 passes at the velocity indicated in (A). The images in (E) and (F) were obtained at 10000 \times magnification. Scale bar = 500 nm.

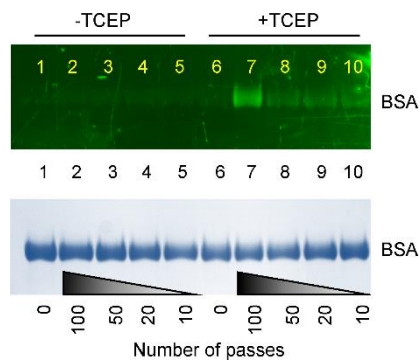


Figure S13: Analysis of stressed BSA incubated with IAEDANS dye *ex situ*. Top image shows the gel excited by UV light provided by a UV-trans illuminator. Bottom image is the same gel stained with Coomassie Brilliant Blue. A 5 mg mL⁻¹ BSA solution was stressed for 0 – 100 passes in the presence or absence of 0.5 mM TCEP at a plunger velocity of 8 mm s⁻¹ (strain rate = 11750 s⁻¹). The IAEDANS was added after a relaxation period.

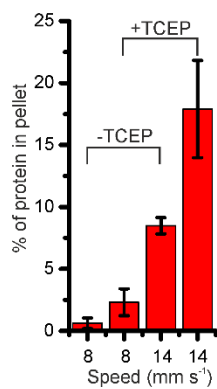


Figure S14: Percentage of insoluble BSA after extensional flow in the presence or absence of reductant. Percentage of insoluble material following extensional flow stress of 5 mg mL⁻¹ BSA for 100 passes at plunger velocities of 8 or 14 mm s⁻¹ (strain rates = 11750 and 20481 s⁻¹, respectively) in the absence (-TCEP) or presence (+ TCEP) of 0.5 mM TCEP. Error bars represent the error from two independent experiments.

Table S1: Values associated with the experimental flow field. These values are assumed constant unless otherwise stated.

Entity	Value
Syringe diameter	4.61 mm
Capillary diameter	0.3 mm
Plunger velocity	8 mm s ⁻¹
Velocity in capillary	1.9 m s ⁻¹
Volumetric flow rate	0.13 mL s ⁻¹
Reynolds number (syringe)	37
Reynolds number (capillary)	570
Centre line strain rate	11750 s ⁻¹
Centre line shear rate	52000 s ⁻¹

Table S2: The number of peaks and their corresponding mean hydrodynamic radii (nm) obtained by regularization analysis of DLS data for 1, 2, 5 and 10 mg mL⁻¹ BSA subjected to extensional flow. The protein solutions were at a plunger velocity of 8 mm s⁻¹ (strain rate = 11750 s⁻¹ and shear rate = 52000 s⁻¹). Particles larger than 5 μm are outside the accurate limits of size determination for DLS, but are shown for completeness (4).

Protein Conc.	No. of passes	Peak 1 (nm)	Peak 2 (nm)	Peak 3 (nm)	Peak 4 (nm)
1 mg mL ⁻¹	0	3.4 ± 0.9			
	10	3.1±0.6	1748±434		
	20	3.3±0.9			
	50	3.2±0.8	5955±2106		
	100	3.5±1.2	310±80		
	500	3.3±0.66	77±25	994±357	
	1000	7.0±5.7	14225±11450		
	1500	5.2±24	16490±16460		
	2000	3.0± 0.5	139± 20	1915± 576	140564 ± 172260
2 mg mL ⁻¹	0	3.3±1			
	10	3.2±0.7			
	20	3.2±0.8			
	50	2.9±0.8	857±812	367715±237351	
	100	2.2±0.6	98±32	693±227	16215 ±5780
	500	4.1±1.1	887±705	26911±12802	
N =1	1000	11.2±3.8	58522±129872		
	1500	4.4± 2.2	24678±29920		
	2000	8.4±1.6	1230±571	27912±12189	
5 mg mL ⁻¹	0	3.2±0.8			
	10	3.4±1.0	506±157		
	20	3.3±0.8	292±76		
	50	3.1±0.6	2146±700	52739±24392	
	100	2.5±0.9	36±9	31158±7720	
	500	3.2±1	352±100	37600±8400	
	1000	4.6±1.4	22636±34198		
	1500	4.2±2.6	13983±20580		
	2000	3.7±0.8	82±21	26683±39806	
10 mg mL ⁻¹	0	3.3±1.0			
	10	3.3±0.9			
	20	2.7±0.3	15598±4812		
	50	2.4±0.3	520±140	3713±1268	
	100	2.9±1.1	5877±12817		
	500	3.5±0.9	65±9	12383±12494	
	1000	2.8±0.5	26±5	2896±2044	65301 ±23533
	1500	3.7±1.7	531±441	12722±5140	
	2000	5.4±1.3	15623±33429		


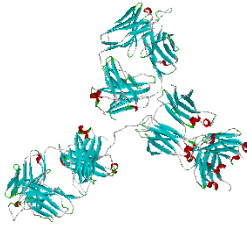
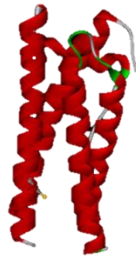
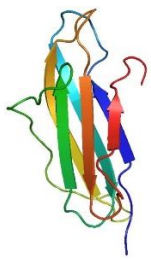
Table S3: The polydispersity index (PDI) of 1, 2, 5 and 10 mg mL⁻¹ BSA after 0-2000 passes at a plunger velocity of 8 mm s⁻¹ (strain rate = 11750 s⁻¹ and shear rate = 52000 s⁻¹). PDIs were calculated from the z-average radii and distribution widths shown in Figure S6.

	PDI	z- average radius (nm)	PDI	z- average radius (nm)	PDI	z- average radius (nm)	PDI	z- average radius (nm)
Number of passes	1 mg mL ⁻¹		2 mg mL ⁻¹		5 mg mL ⁻¹		10 mg mL ⁻¹	
0	0.16	3.6	0.14	3.5	0.13	3.5	0.13	3.5
10	0.22	3.5	0.09	3.5	0.26	3.6	0.19	3.4
20	0.16	3.5	0.12	3.5	0.25	3.5	0.23	3.4
50	0.27	3.5	0.58	259.2	0.34	4.0	2.19	39.6
100	0.3	3.6	2.66	66.7	0.39	4.4	0.08	208.4
500	1.49	9.4	1.56	153.2	0.88	5.2	2.84	158.4
1000	1.47	366.7	0.71	26.6	1.75	177.4	1.55	26.7
1500	1.65	530.1	0.81	641.6	2.42	156.5	1.94	71.9
2000	2.39	47.4	2.11	185.3	2.0	87.9	1.83	214.4

Table S4: Hydrodynamic radii obtained by fitting the FCS data shown in Figure S7.

No. of passes	Mean R_h (nm)			
	1 mg mL ⁻¹	2 mg mL ⁻¹	5 mg mL ⁻¹	10 mg mL ⁻¹
BSA	5.0	5.2	2.7	4.2
10	16.5	16.4	8.8	7.3
20	27.6	15.6	23.3	21.3
50	40.6	47.5	34.9	146.7
100	53.7	98.7	52.0	223.3
500	101.3	17.5	256.8	17.2
1000	1280.2	1029.7	3089.4	1024.2
1500	1204.0	12492.8	3403.0	2921.8
2000	6007.9	18328.9	4603.2	5890.2

Table S5: Summary of protein characteristics.

	BSA	mAbs	G-CSF C3	β_2m
Amino acids	583	~1400	175	100
MW (kDa)	66	148	18.8	11.86
Size (nm)	3.5	6	2.5	2.3
pI (25 °C)	4.7	mAb1 9.42 WFL 8.64 STT 8.64	5.65	6.05
Structure				
PDB Code:	3V03	1HZH	1RHG	2XKS
ϵ_{280} ($M^{-1} cm^{-1}$)	43824	mAb 1 = 207360 WFL = 239440 STT = 228440	10220	20065

References

1. Yadav S, Shire SJ, & Kalonia DS (2011) Viscosity analysis of high concentration bovine serum albumin aqueous solutions. *Pharm. Res.* **28**:1973-1983.
2. Aris R (2012) *Vectors, Tensors and the Basic Equations of Fluid Mechanics* (Courier Corporation).
3. Jaspe J & Hagen SJ (2006) Do protein molecules unfold in a simple shear flow? *Biophys. J.* **91**:3415-3424.
4. Hassan PA, Rana S, & Verma G (2015) Making Sense of Brownian Motion: Colloid Characterization by Dynamic Light Scattering. *Langmuir* **31**:3-12.
5. Hanlon AD, Larkin MI, & Reddick RM (2010) Free-solution, label-free protein-protein interactions characterized by dynamic light scattering. *Biophys. J.* **98**:297-304.
6. Roger V, Cottet H, & Cipolletti L (2016) A New Robust Estimator of Polydispersity from Dynamic Light Scattering Data. *Anal. Chem.* **88**:2630-2636.
7. Gell C, *et al.* (2008) Single-molecule fluorescence resonance energy transfer assays reveal heterogeneous folding ensembles in a simple RNA stem-loop. *J. Mol. Biol.* **384**:264-278.
8. Tipping KW, *et al.* (2015) pH-induced molecular shedding drives the formation of amyloid fibril-derived oligomers. *Proc. Natl. Acad. Sci. USA* **112**:5691-5696.
9. Gell C, Brockwell D, & Smith A (2006) *Handbook of Single Molecule Fluorescence Spectroscopy* (Oxford University Press, Oxford).
10. Mukaiyama A, *et al.* (2013) Native-State Heterogeneity of β 2-Microglobulin as Revealed by Kinetic Folding and Real-Time NMR Experiments. *Journal of Molecular Biology* **425**:257-272.